CHAPTER 4: NEW HIGH RESOLUTION GROUND MAGNETIC SURVEYS IN THE VREDEFORT DOME

The main focus of this dissertation is to present new high resolution geomagnetic data (see also Muundjua et al. 2007) from selected areas in the Vredefort Dome for the purpose of determining (1) variations of the magnetic field across the contacts of different geological units, (2) whether the various geological units have distinct magnetic signatures, (3) how the presence of deformation features affects the magnetic field, (4) how the ground magnetic data correlate with available aeromagnetic data (using an upward continuation algorithm), (5) how the results correlate with findings of palaeomagnetic data in the same area, and (6) two and three-dimensional models of the magnetic anomaly across the Vredefort basement.

To meet the above objectives three sets of geomagnetic surveys were conducted: (1) a detailed survey over the transition zone, (2) a more closely spaced survey over outcrops of BIF and (3) a very detailed survey over a 9 m x 9 m grid in the granulite terrain. Objectives relating to the geomagnetic survey are dealt with in this chapter. Those pertaining to palaeomagnetic data and modelling will be dealt with in Chapter 5 and 6 respectively.

4.1 Detailed survey over the transition zone

Fig. 4.1 shows the positions and magnetic values of the survey points over the study area. Blank spaces in Fig. 4.1 are inaccessible areas like lakes, rivers and settlements. The average spacing of survey lines was ~25 m (Fig. 4.1). Based on the daily base station readings it was found that the diurnal variations over the duration of the survey period were between about 20 nT/day and 100 nT/day. These values were found to be insignificant compared with the variation of the observed data (10550 nT to 75450 nT). Therefore, the data were not corrected for diurnal variations. Of the 320 000 data points recorded, 63 fell outside the sensitivity of the instrument (between 17000 to 90000 nT) and these were discarded in the final anomaly map. The maximum gradients measured were about 9000 nT/m.

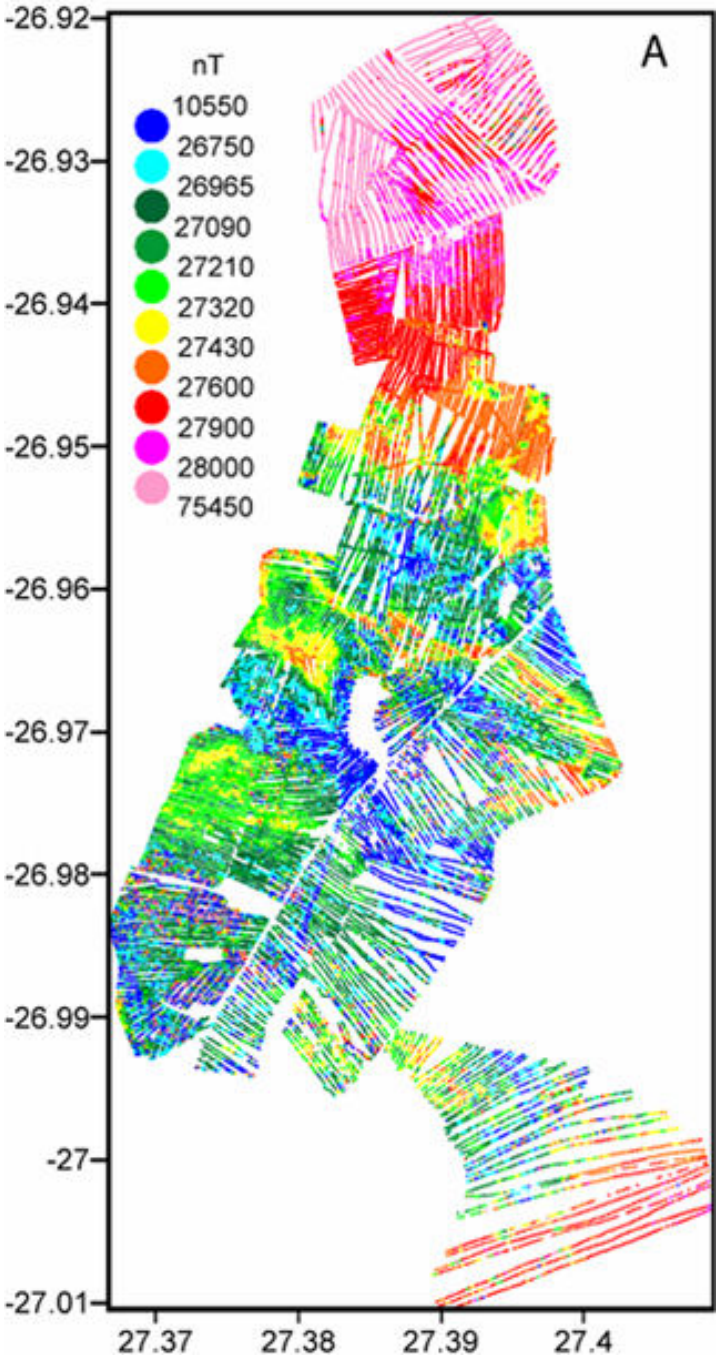

Figure 4.1. Line spacing and magnetic intensity for the detailed ground magnetic survey across the amphibolite-granulite transition (station spacing 1-15 m, line spacing ~25 m, sensor height 2 m). Each point on this diagram represents the measured position and the corresponding raw magnetic values, measured directly with the cesium magnetometer. Note that values which fell out of the accepted range of the magnetometer were removed. The blank areas are roads, dams, buildings or settlements. The 63 values that fell out of the range of the sensitivity of the instrument (those below 17000 nT) are still part of this map. The x–axis and y-axis are longitude E and latitude S respectively.

The magnetic anomaly map (Fig. 4.2) was determined by subtracting the IGRF field (Maus et al., 2005) from the observed data. The 2005 IGRF field calculated at the centre of the survey grid (latitude, -26.962^{o}S; longitude, 27.387^{o}E; altitude, 1500 m) yields the following values: declination, -18.5^{o}; inclination, - 63.75^{o}; total intensity, 28167 nT. The interpolation of the anomaly map (Fig. 4.2) was obtained using a grid lattice of 9 x 9 m. In order to obtain reasonable contrasts in the anomaly map, the maximum and minimum values were set to between 0 and -2000 nT respectively. These values are not absolute, as the use of the absolute values will not yield a good presentable map.

From the IGRF anomaly map (Fig. 4.2), a number of general observations can be made. The extreme northern and southern ends of the map are characterised by magnetic fields that approach the Earth's ambient field. Magnetic fields become progressively more negative toward the transition zone, reaching a minimum of about -2000 nT close to the centre of the transition. There are alternating bands of relatively more and less negatively magnetized regions that roughly strike NW. A thin (~50 m wide) NNE trending linear feature (A-B, Fig. 4.2) is readily observed and cuts across the entire central part of the map. There is also an abrupt change in magnetic field strengths along a NW–trending lineament (C-D, Fig. 4.2). Superimposed on the regional trends are relatively short wavelength variations that are more pronounced within the transition zone and also in the south-western sector of the surveyed area (Fig. 4.2).

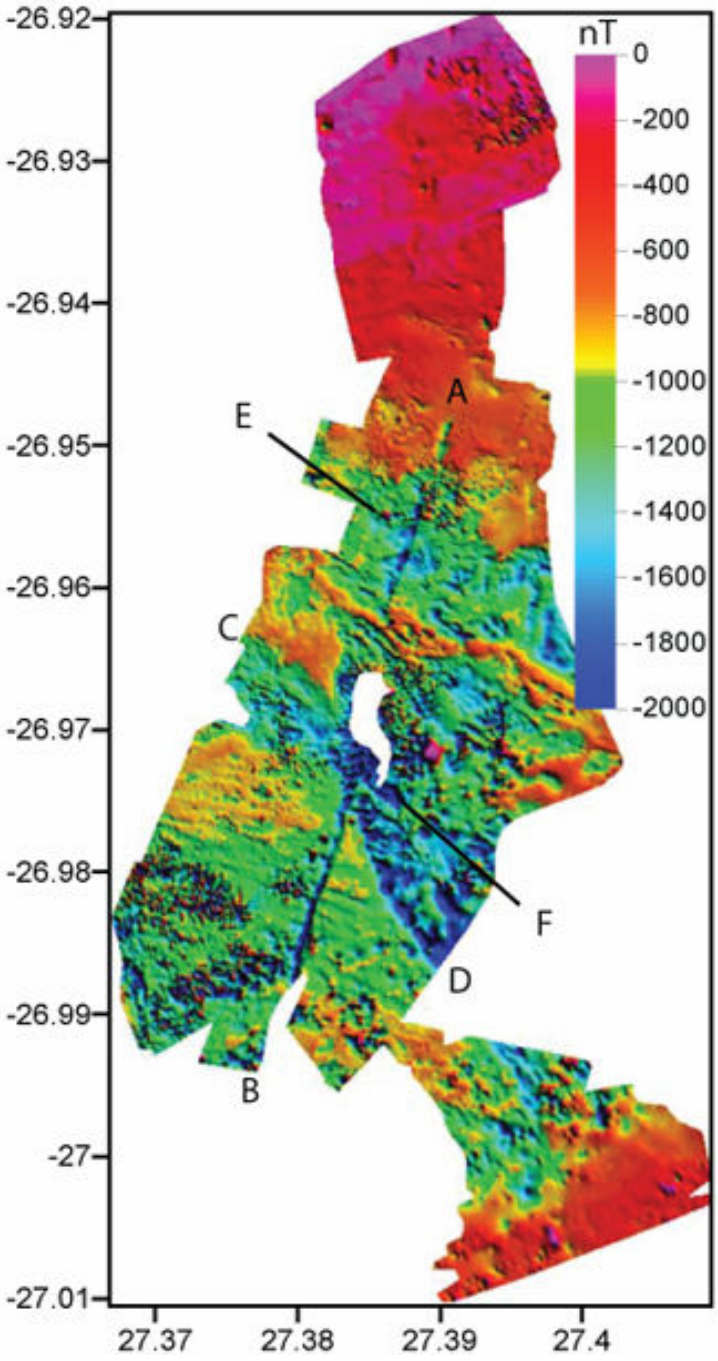

Figure 4.2. Detailed IGRF-corrected ground magnetic anomaly map over the amphibolite-granulite transition gridded to 9 x 9 meters. A-B and C-D show the positions of lineaments discussed in the text, and E and F show the localities of the BIF and 9 x 9 square metre grid respectively.

4.1.1 Correlation of magnetic anomalies with the geology

The magnetic survey over the amphibolite-granulite transition (Fig. 4.2, Fig. 4.3 and Fig. 4.4) shows a broad correlation with the geological map (Fig. 1.3, Chapter 1). The N-S profile (Fig. 4.4a) shows a gradual decrease in the magnetic field over the Outer Granite Gneiss towards the amphibolite-granulite transition reaching a minimum in the mixed charnockite and granite–gneiss zone that constitutes the transition. The magnetic field then increases southwards away from the transition zone, towards the centre of the crater reaching values equivalent to the Earth's ambient field about 2 km into the granulite terrain.

Comparing the geology and the magnetic signal along all of the sections shown in Fig. 4.4 suggests that there is no lithology that gives a distinct magnetic signature, and it appears that both long wavelength and short wavelength signals are not confined to any one particular lithology. However, there does appear to be a change in amplitude over some of the lithological boundaries, as seen particularly along the N-S and NW-SW profiles (Fig. 4.4a and 4.4b). Furthermore, the NW striking magnetic patterns, particularly north of the transition zone, roughly follow the strike of the geological units (Fig. 1.3, Chapter 1), but this phenomenon is not so evident in the eastern part of the map. The abrupt change in magnetic field strengths along the NW–trending lineament (C-D, Fig. 4.2) correlates with the NW-trending impact-related radial fault (Fig. 4.2 and Fig. 1.3).

It appears that the boundaries of the major domains (OGG, transition zone, ILG), needs to be shifted as suggested in Fig. 4.4a (profile 1). A detailed geological study, more detailed interpretation of these data could more precisely delineate the transition zone and its subdivisions. A complete geomagnetic investigation (taking into account the diurnal variations) should involve a geological interpretation of the data and follow-up geological field work. However, a new interpretation of the geological map is beyond the scope of the current study and will be the subject of a subsequent investigation. It must be noted that rock outcrops are poor and this will make any ground truthing a difficult task.

Despite concerted efforts in the field, no surface geological exposure was found that could account for the NNE–trending lineament (A-B, Fig. 4.2). The southern part of this lineament closely corresponds to a buried water pipe that was laid to bring water from the Vaal River to the town of Vredefort. However, the pipe is made of asbestos cement, and turns away from the lineament along the main road to Parys and therefore cannot account for the lineament. This feature does not appear to be offset by the NW trending fault (C-D).

Another important observation is that there is no appreciable magnetic contrast between the impact melt dyke and pseudotachylites compared with the surrounding basement rocks (this study). These features occur in small patches and it will be difficult to show on this diagram. However, these observations are based on separate localized surveys that the author conducted at localities where the impact melt dykes and pseudotachylites are exposed.

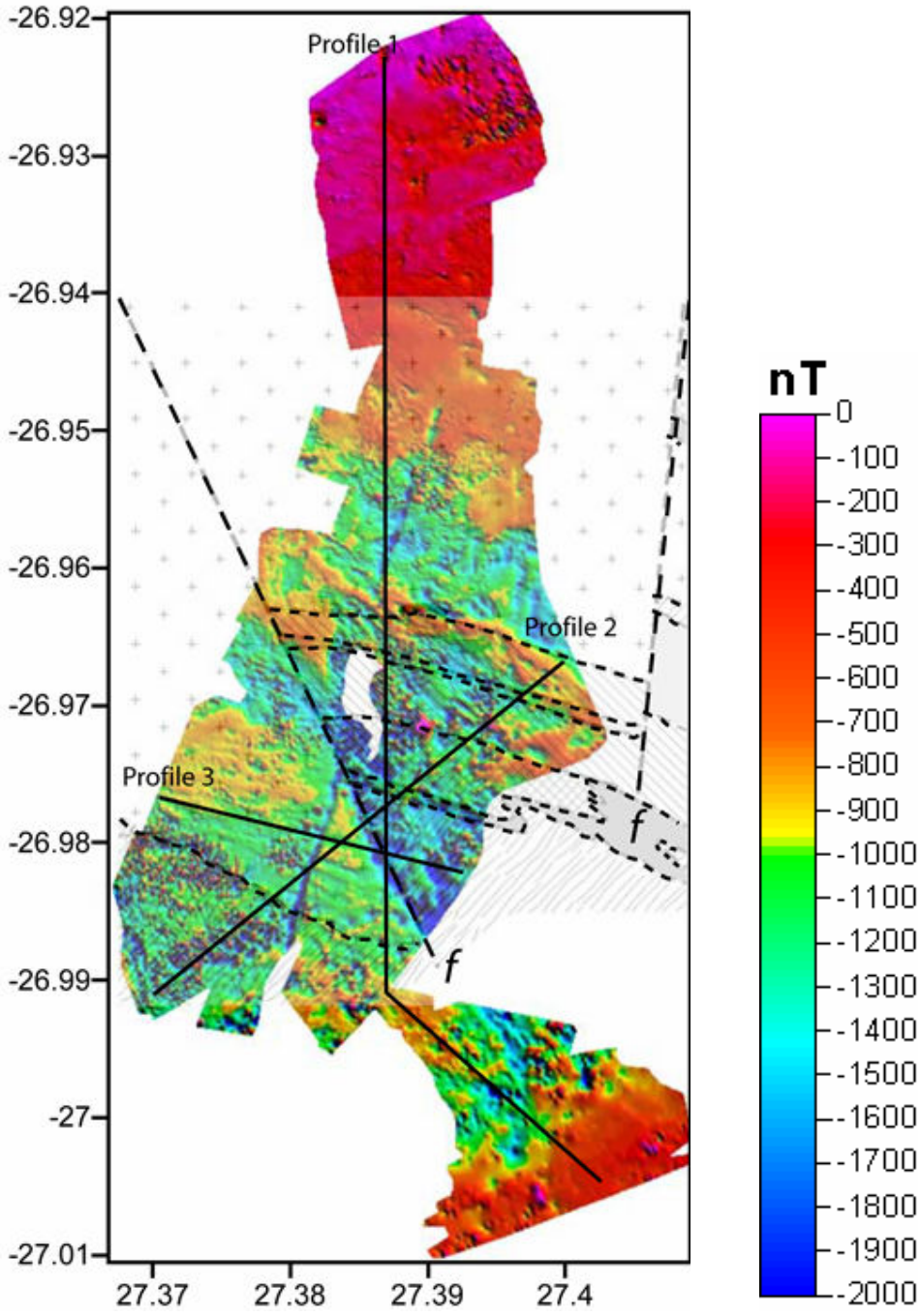

Figure 4.3. Geology (see Chapter 1) of the region superimposed on the IGRF magnetic anomaly map and the positions of profiles 1 to 3 from which two-dimensional anomalies were derived (see Fig. 4.4).

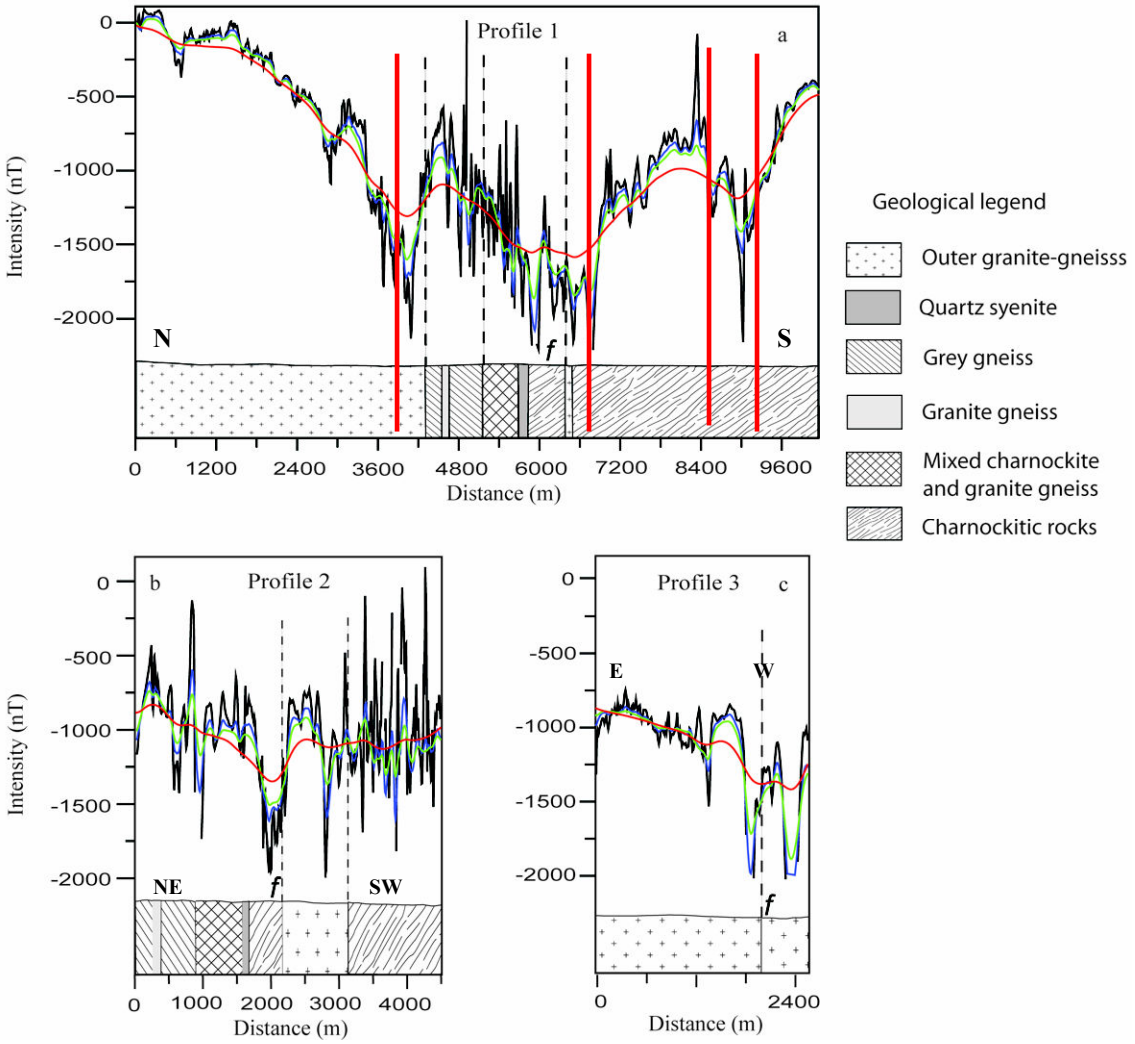

Figure 4.4. Magnetic profiles for traverses shown in Fig. 4.3 and their corresponding upward continued profiles (at 20, 40 and 150 metres) compared with cross-sections through the underlying geology. The colour code is as follows: black is raw data, blue is data at 20 m height, green is data at 40 m height, and red is data at 150 m height. Each profile starts from the labelled end shown in Fig. 4.3. The red vertical lines across profile 1 indicate the new interpreted position of the transition zone as well as an intrusive rock within the charnockitic rocks towards the south of the profile.

4.1.2 Upward continuation of field data

The application of the upward continuation filter reveals large-scale regional anomaly patterns because short wavelength anomalies are smoothed out while long-wavelength anomalies are retained (Chapter 3). The purpose of applying the filter to the current data set was to 1) to compare the results with the geology, 2) obtain an upward-continued grid that can be compared directly with the aeromagnetic data set over the same area, and 3) select upward-continued data of a suitable wavelength for subsequent modelling (Chapter 6) by removing wavelengths that correspond to anomalies less than those of interest in the interpretation.

Figs. 4.4a to 4.4c show a series of magnetic profiles through the survey grid taken from the IGRF corrected data and their upward continued profiles. Corresponding upward continued maps are shown in Fig. 4.5. These profiles where chosen because they cut across most of the lithology. Most of the high frequency signals disappear at a height of 20 metres. The remaining signals (of the 20 m upward continued profile) consist of medium wavelengths in the range of 20 m to100 m with amplitudes from 200 nT to 800 nT, and some longer wavelengths (up to 3000 m) with amplitudes of 100 nT to 600 nT.

Fig. 4.5c (map) and Fig. 4.6 (profiles) show the upward-continued data at 150 m, which corresponds to the elevation of the aeromagnetic survey. Fig. 4.5d shows the aeromagnetic data that coincide with Fig. 4.5c. As expected, short-wavelength anomalies are suppressed for the 150 m upward continued and the aeromagnetic data compared with ground data. Furthermore, the general anomaly-pattern in the 150 m upward continued data is very similar to that seen in the aeromagnetic data. The profiles in Fig. 4.6 indicate that the 150 m upward continued data contain more detailed anomalies than the aeromagnetic data, and this is probably due to the wider sampling interval along the lines used in the aeromagnetic data. The match between the two data sets is very good which suggests that the data from the current study and the aeromagnetic data are compatible.

A check on the quality of the data is illustrated in Fig. 4.7, which shows the variance of the data for each data set (raw and upward continued data). The formula used for calculating the variance is commonly known formula found in most basic mathematics textbooks. Below is the formula for calculating the variance:

$$\delta^2 = \frac{1}{N}\sum_{i=1}^{N}(x_i - \bar{x})$$

Where N is the size of the data, and $\bar{x}$ is the mean of the data.

The figures were obtained by calculating the variance in a 70 m x 70 m window throughout the data set. The variance is here loosely used to approximate the noise in the data. The "noise estimates" illustrate the effectiveness of upward continuation in successfully removing noise from the data. However, the advantage of removing noisy signals is traded against losing other valuable shorter wavelength signals.

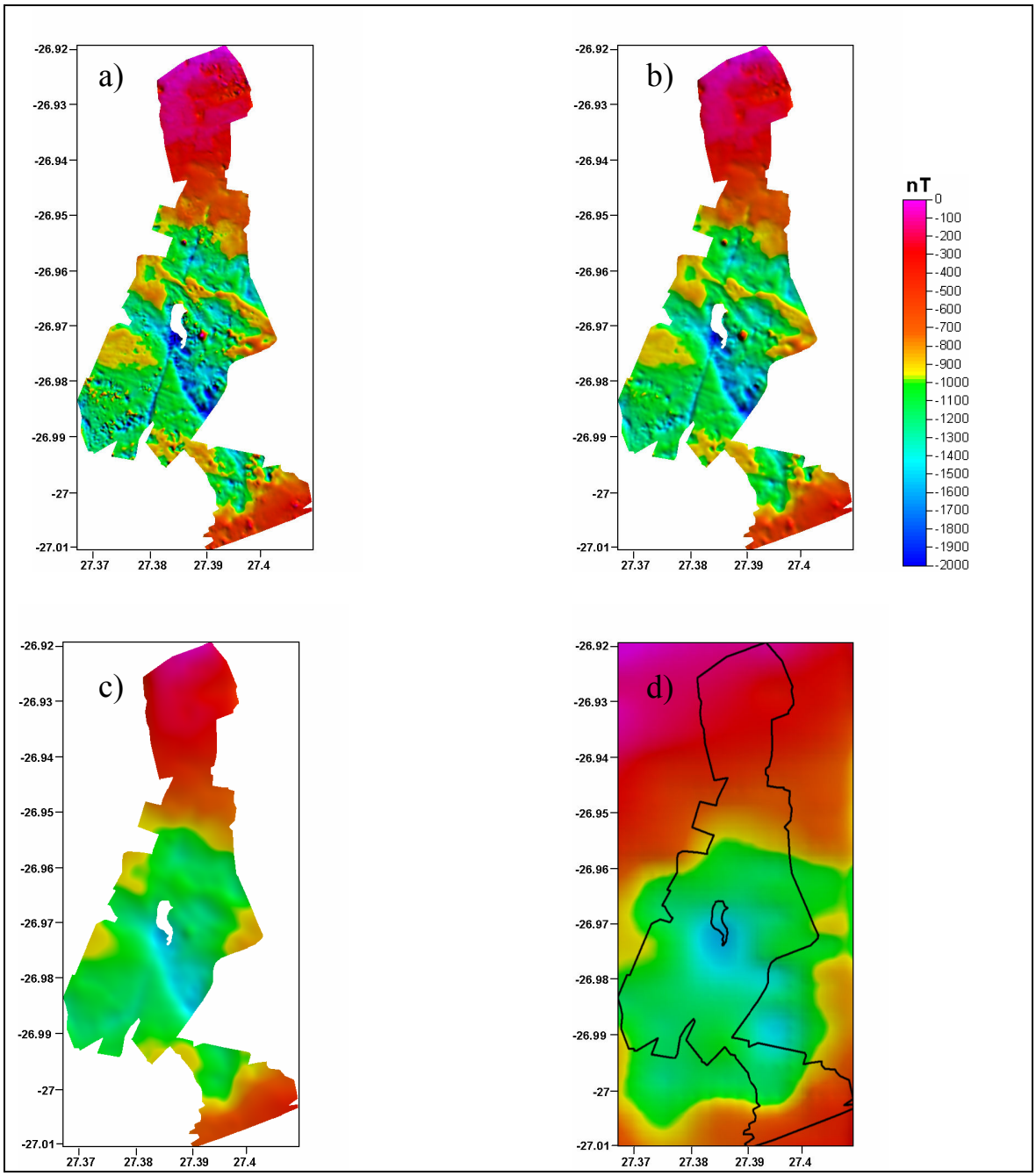

Figure 4.5. Upward continued data to a) 20 m, b) 40 m and c) 150 m. d) Portion of the aeromagnetic data, showing the outline of the current study area for comparison with upward continued data. Note that the intensity (nT) scale applies to all four diagrams.

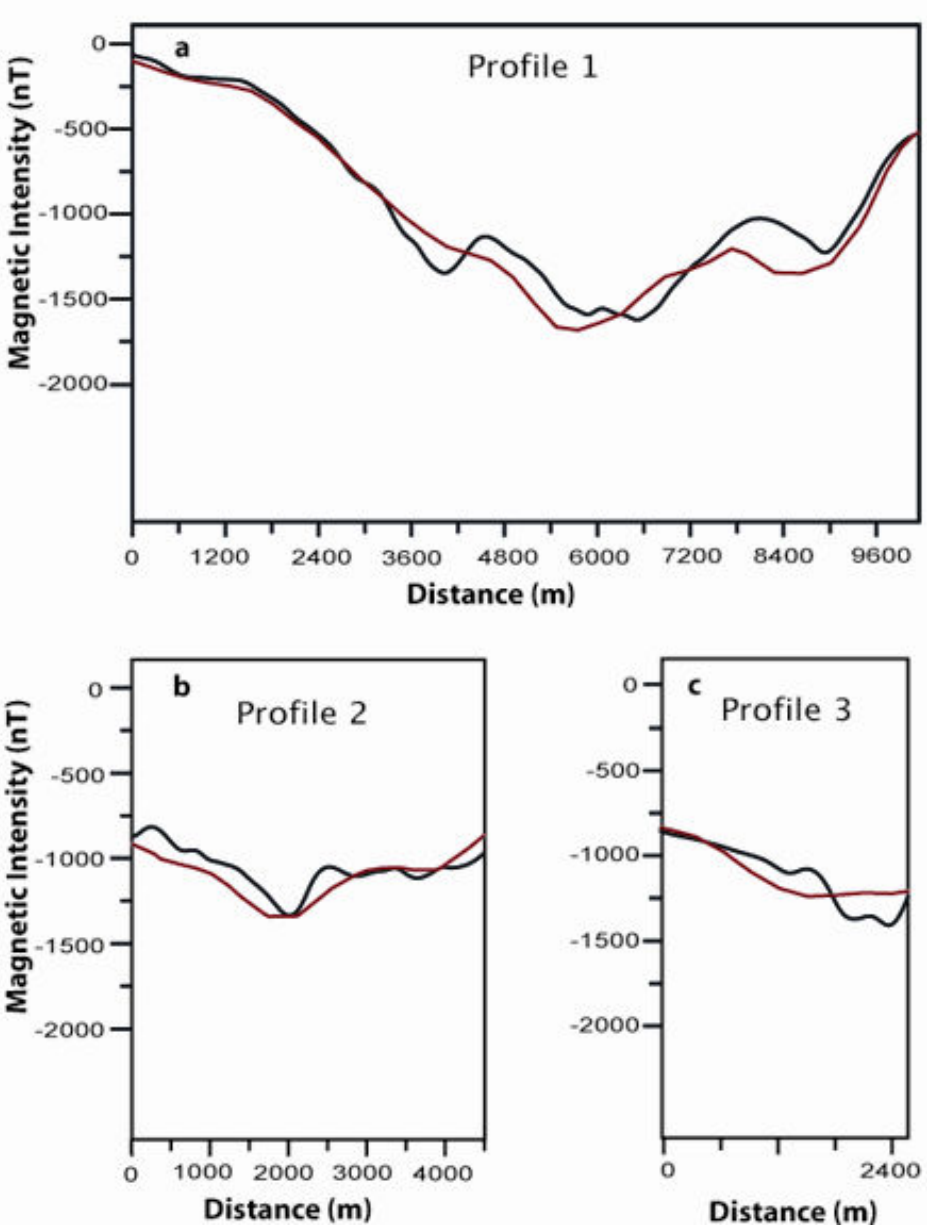

Figure 4.6. Comparison of the upward continued profiles (150 m, shown in black) from Fig. 4.3 and their corresponding aeromagnetic profiles (shown in red). Each profile starts from the labeled end shown in Fig. 4.3.

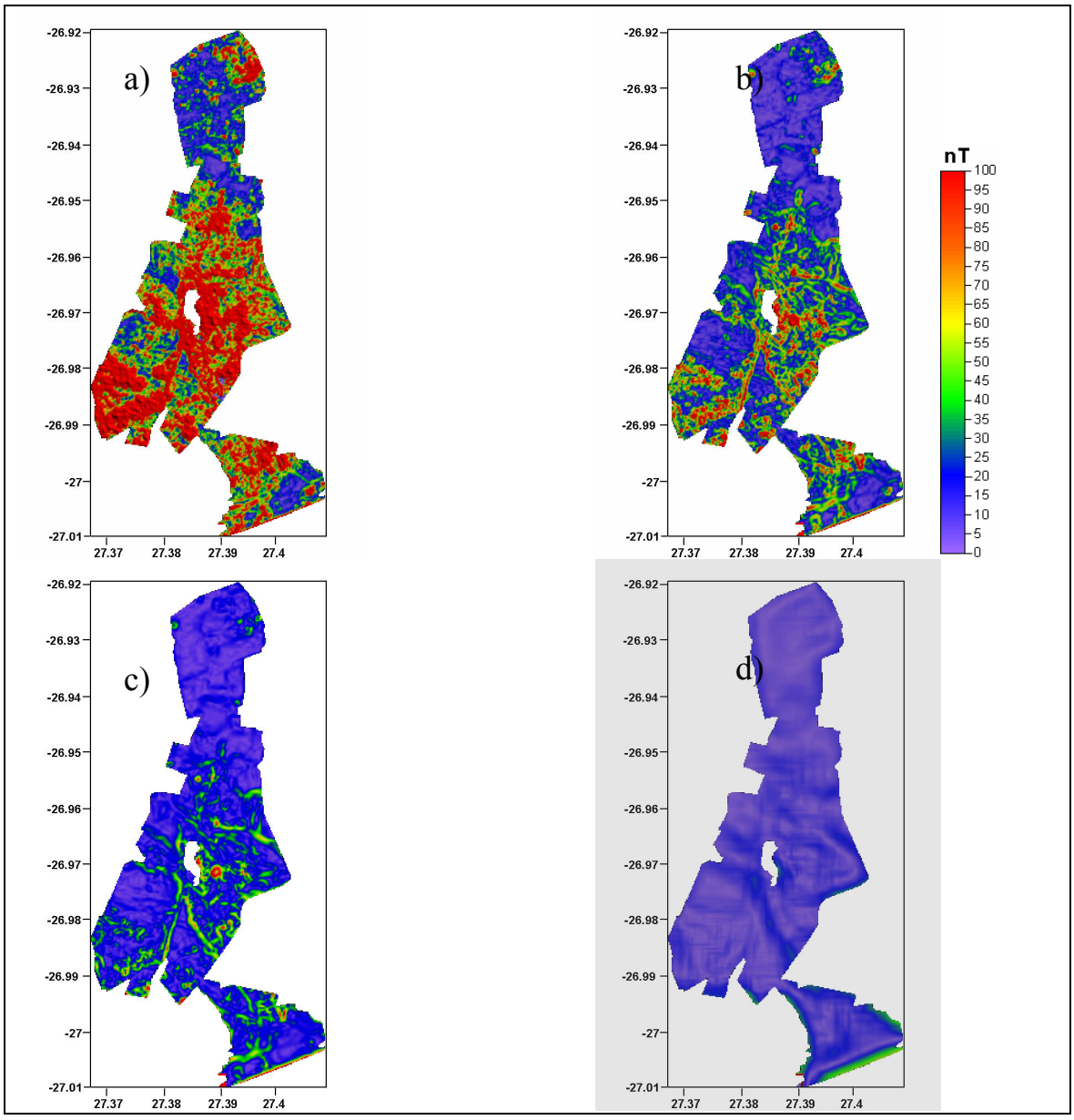

Figure 4.7. Calculated variance of the magnetic data. a) Raw data, b) data upward continued to 20 m, c) data upward continued to 40 m and d) data upward continued to 150 m. The variance was calculated by passing 70 m x 70 m window throughout the data set. Note that the intensity (nT) scale applies to all four diagrams.

4.1.3 Automatic gain control of field data

For image enhancement, the area of interest is the middle part of Fig. 4.8 which coincides with the amphibolite-granulite transition zone. By highlighting any underling features

and enhancing some of the subtle ones, magnetic patterns that are not easily visible can be revealed. For this purpose a data set (red square in Fig. 4.8) was extracted for analysis using the AGC filter.

AGC was applied using a variety of window sizes (Fig. 4.9). To make the discussion of the data easy a number of specific features throughout the area, which will mostly be referred to in the analysis are labeled with letters A-I (Fig. 4.9). The best results (whereby most subtle features were highlighted, feature A and B) were obtained when a window size of 21 x 21 (200 m x 200 m in ground units) was used (Fig. 4.9b) of the chosen window sizes. Increasing the window size to 51 x 51 (500 m x 500 m in ground units, Fig. 4.9c) and 201 x 201 (2000 m x 2000 m in ground units, Fig. 4.9d) one sees that fewer anomalies are enhanced with respect to the original data (Fig. 4.9a).

However, Figs. 4.9b and 4.9c highlight a number of interesting points. The images show good quality enhanced linear features, and accentuate other smaller details (between linear feature D and J). The linear features in Fig. 4.9b were drastically improved compared with Fig. 4.8, therefore making comparison with geology easier (linear feature D). Lineaments with weaker signals are clearly visible in some of the diagrams (Fig. 4.9b and c). Throughout the AGC enhanced maps subtle features are ubiquitous (compare Fig. 4.9a with Figs. 4.9b and c). Some of these might be underlying features which might be correlated to the geology. It is difficult to confirm this either way as geology outcrop is very poor and isolated. It is possible that the plethora of anomalies in some of the AGC maps is noise that can be attributed to the AGC filter itself (in particular the south-east of Fig. 4.9b).

In the upper sections of Fig. 4.9b and Fig. 4.9c in particular, the linear features are easily traceable and they clearly coincide with the different lithologies (see Fig. 1.3, C, D and J). Some anomalies which appear as single anomalies in the raw magnetic data (Fig. 4.2) occur as discontinuities in the AGC filtered maps (Fig. 4.9, see features F, G and H, features C and E and feature I). From Fig. 4.9 it is easier to follow the NE trending lineaments discussed earlier in the text (feature A).

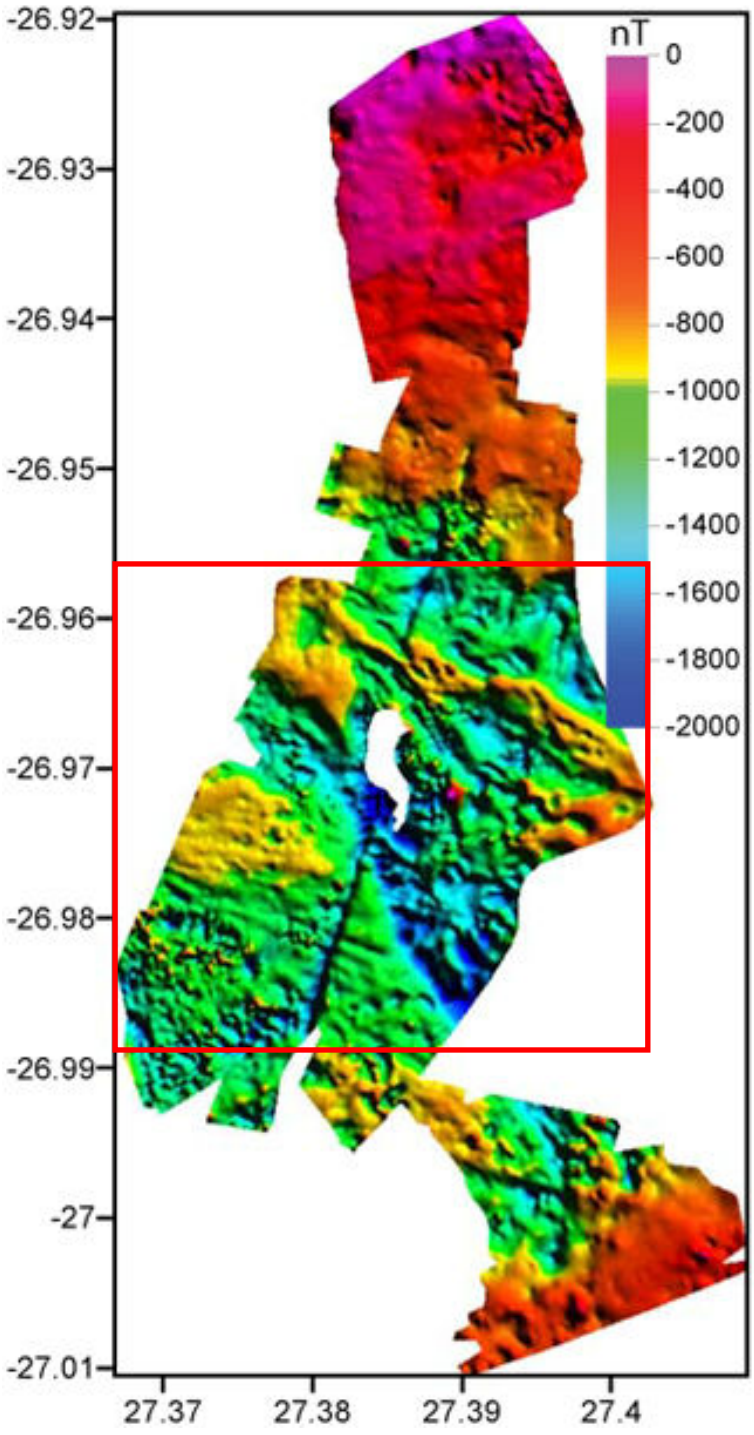

Figure 4.8. Detailed IGRF-corrected ground magnetic anomaly map over the amphibolite-granulite transition gridded to 9 x 9 meters. The red square shows outline of the area used for automatic gain control analysis (see Fig. 4.9 results).

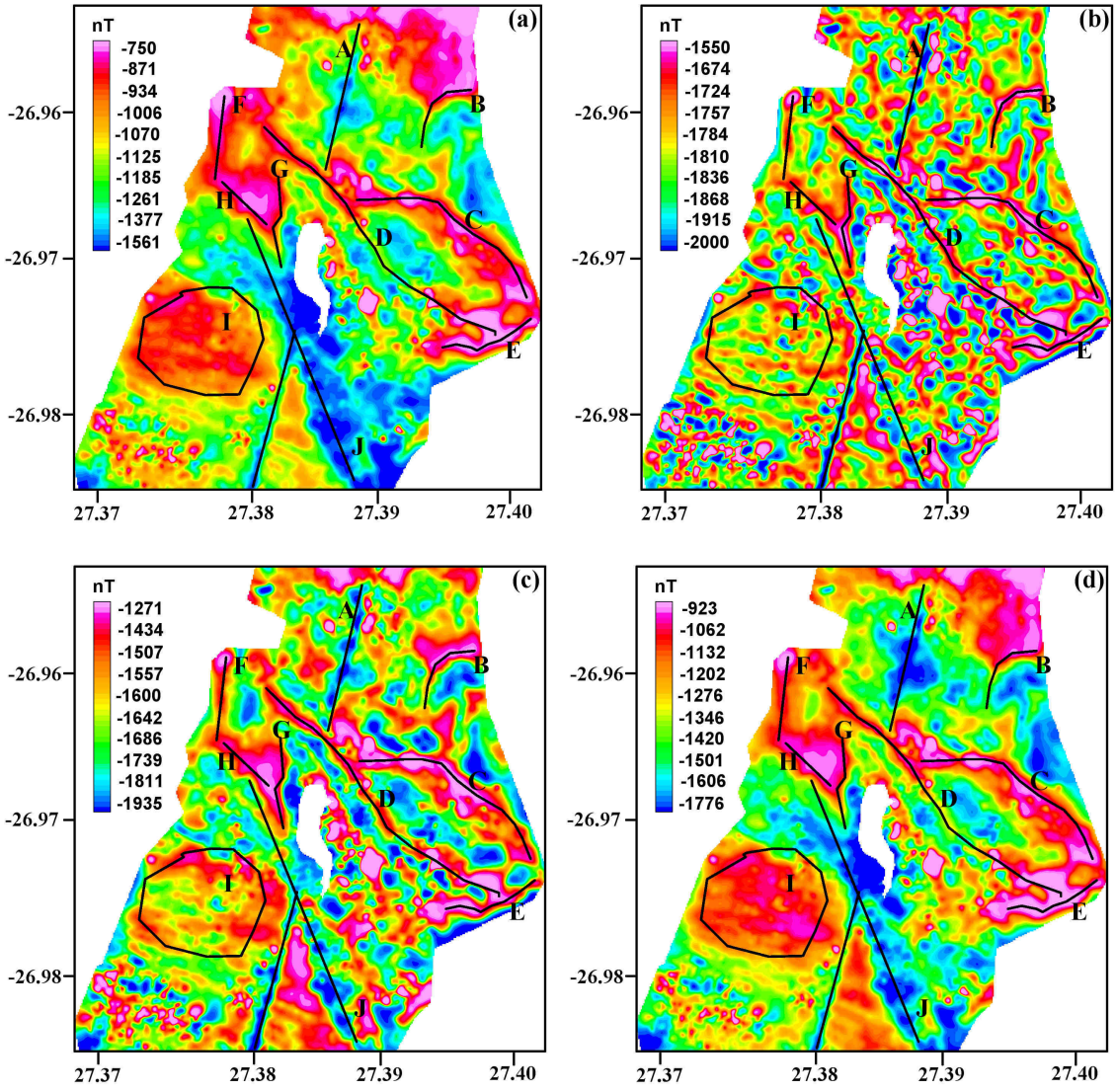

Figure 4.9. Sequence of images illustrating the automatic gain control method for highlighting subtle features. (a) Section taken from the detailed IGRF anomaly map (area a Fig. 4.8). (b) AGC method applied to (a) using an 21 x 21 window. (c) AGC method applied to (a) using a 51 x 51 window. (d) AGC method applied to (a) using a 201 x 201 window. The features labeled A-I are used to in the analysis in order to gauge the effectives of filter, see text for discussions.

4.1.4 Depth estimate of selected profiles over the south end of NE-trending lineament

The southern-end of the NE-trending linear feature coincides with a water pipe as noted in the text earlier and the calculations will be conducted to see if they give realistic values for a water pipe. A total of five profiles (Fig. 4.10) across the NE trending lineament were selected for depth estimation. The depth estimation was conducted in order to constrain the depth of the source body. Before any analysis could be performed the contribution of the surrounding rocks was removed. This was accomplished by subtracting a constant base value of about 1200 nT.

The Euler deconvolution solutions were generated with the aid of a Matlab program written by G. Cooper of the University of the Witwatersrand, while the wavenumber method was written in Matlab by the author.

The solutions of the depth estimates for profile 1 are shown in Fig. 4.11 and results for this and the other profiles summarized in Table 4.1. The Euler solutions were obtained by using structural indices (SI) of 1 since the anomaly is linear (Reid et al., 1990). The depth estimate for SI = 1 gives an average depth of 18 ± 2.0 m and this is shown in the clustering of solutions (enclosed by the black circle) in Fig. 4.12 for profile 1.

The average depth solution using the wavenumber method is 18 ± 7.1 and this is similar to the Euler method with a structural index of 1.

If the anomaly is due to a water pipe it is very unlikely that it would be buried at a depth of 18 m. Either the depth solutions are wrong and they should not be relied on or the anomaly is not due to a pipe.

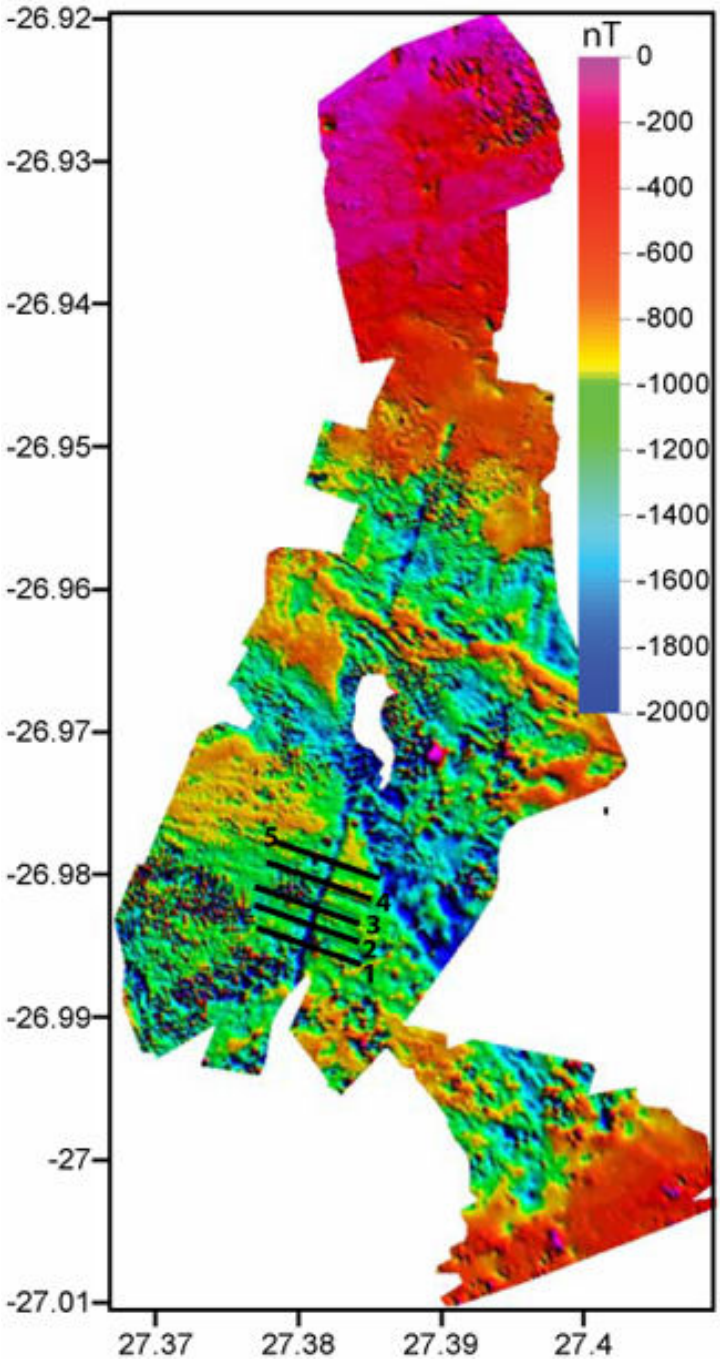

Figure 4.10. Detailed IGRF-corrected ground magnetic anomaly map over the amphibolite-granulite transition showing the 5 profiles across the NE trending lineament that were selected for depth estimation.

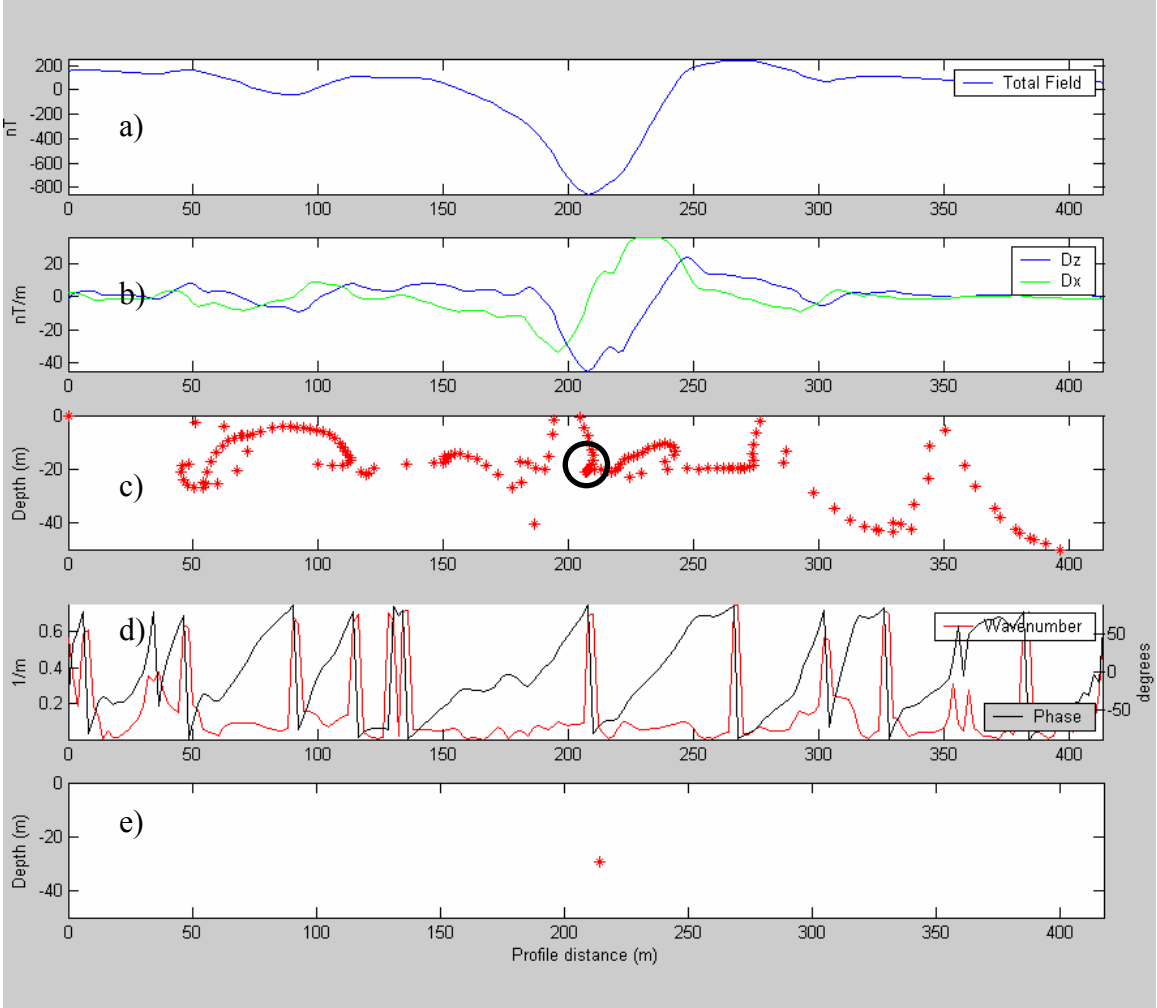

Figure 4.11. Depth estimate for profile 1 across the south end of the NE-SW lineament (Fig. 4.10) using the Euler deconvolution with SI = 1 and local wavenumber methods. (a) Total field anomaly profile extracted from Fig. 4.10 with a constant value of 1200 nT removed (b) Profiles of the vertical and horizontal derivatives of the anomaly. (c) Depth estimates using the Euler deconvolution method (solutions enclosed by the black circles) the estimated depths to the top of the body being 20 m. (d) Profiles of the wavenumber and local phase response. (e) The local depth solution shown as a red dot, yielded depth of 29.6 m.

Table 4.1. Depth determination to top of the south end of the NE-SW linear feature using Euler deconvolution (ED) and the local wavenumber method (LW). The structural index of 1 was used for all profiles in the Euler deconvolution method.

Profile number	Depth (m); ED; SI = 1	LW (m)
1	20.0	29.6
2	16.5	15.0
3	20.2	11.4
4	15.8	20.0
5	17.4	14.6
Average values	18.0 ± 2.0	18.1 ± 7.1

4.2 Very detailed magnetic surveys over the Banded Ironstone Formation (BIF) and the 9 m x 9 m grid

As mentioned earlier, in addition to the main ground magnetic survey, more detailed surveys were conducted over two areas that exhibit particularly high variations of magnetic intensity. The first occurs over a 2000 m^2 outcrop of banded iron formation (BIF) (locality E, Fig. 4.2), and the second is a 100 m^2 survey in the granulite terrain (locality F, Fig. 4.2).

The reason for doing the magnetic survey over the BIF was to determine whether the BIF can be the source of the negative magnetic anomaly which is central to this study. The purpose of the survey in the granulite terrain was to compare the geomagnetic data with palaeomagnetic data (see Chapter 6) and also to permit inversion for the subsurface magnetization.

4.2.1 Results of survey over the Banded Ironstone Formation (BIF)

The survey covered an area of 2000 m^2 and data were collected at a 2 m line spacing using the cesium vapour magnetometer. The sample spacing was about 0.5 seconds yielding an average ground spacing of 0.357 m along lines (see Fig. 4.12).

The IGRF corrected magnetic image over the BIF (Fig. 4.13) consists primarily of positive anomalies with some isolated negative anomalies. The anomalies range in amplitude up to 20 000nT, with an average width of about 12 m. These parameters were determined from all the individual profiles as measured in the field. It appears that the BIF was remagnetised since the time of impact or was not affected by the impact event. If it was affected by the impact event then the predominant anomaly over the BIF should be negative. The signature of the magnetic anomaly associated with the impact event is negative (this study).

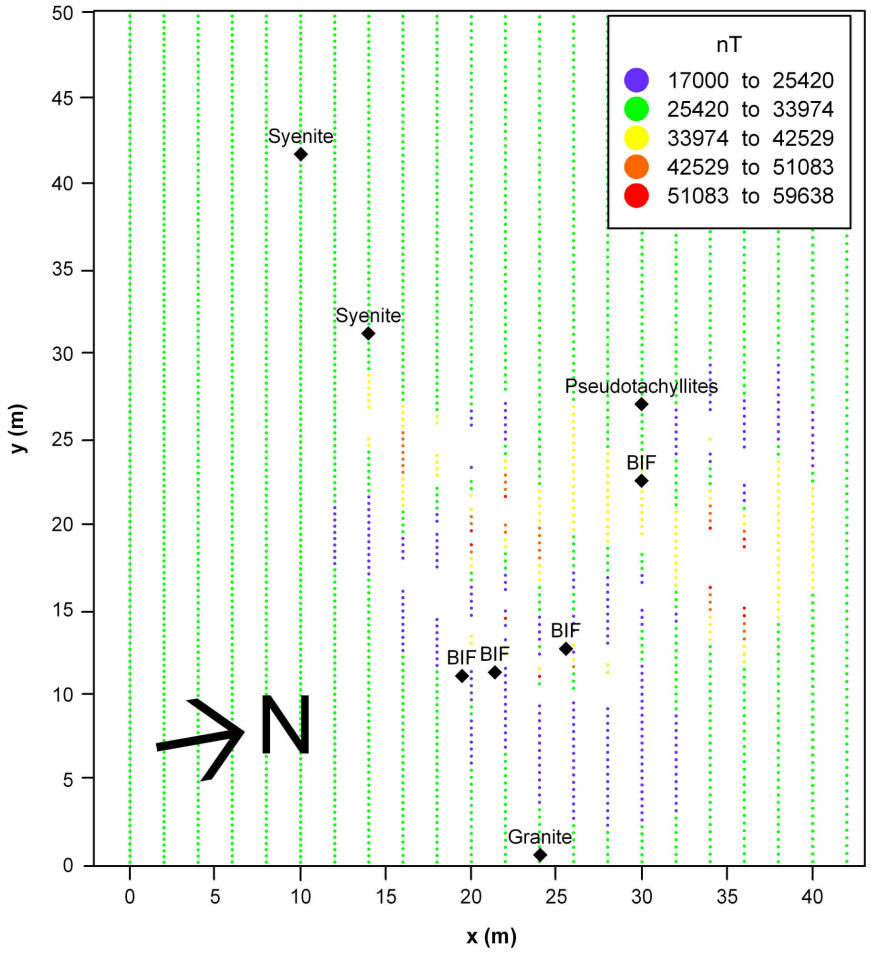

Figure 4.12. Magnetic survey over the BIF (station spacing ~0.357 m, line spacing ~2 m, and sensor height 2 m). Each point on this diagram represents the measured position and the corresponding raw magnetic values. Also shown are the positions of outcrops of different rock types.

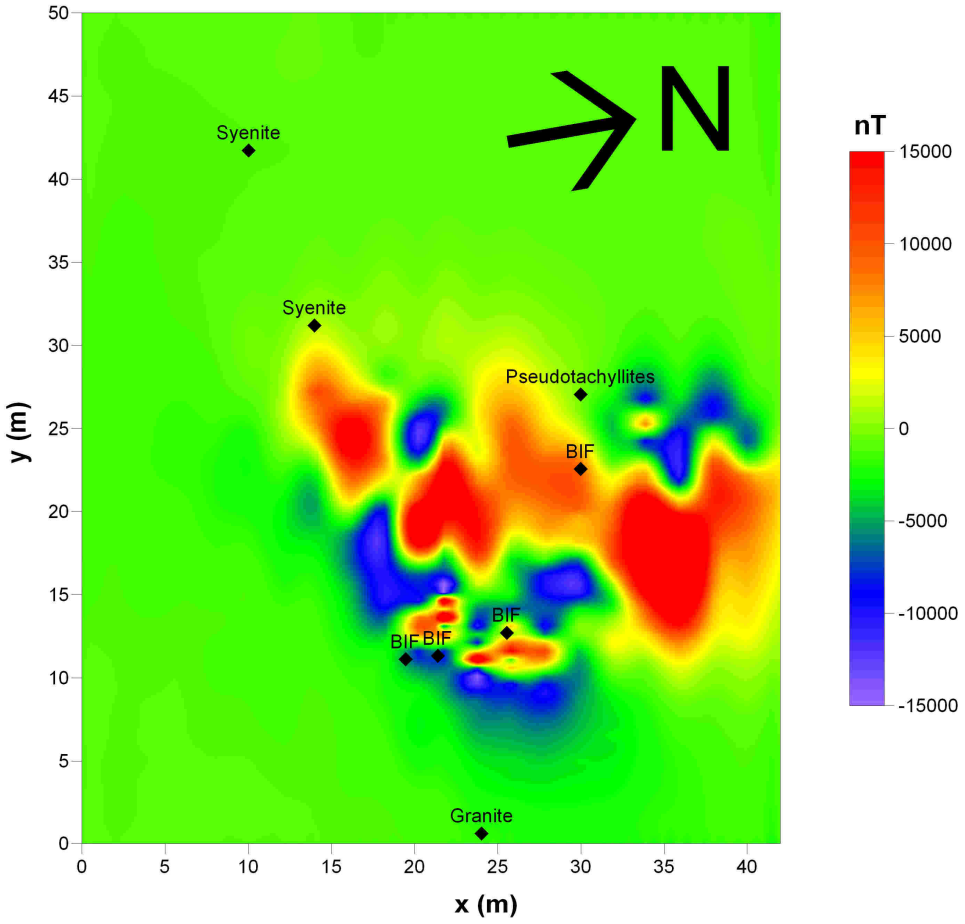

Figure 4.13. IGRF corrected magnetic anomaly map over the BIF. Also shown are the positions of outcrops of different rock types.

4.2.2 Magnetic survey of the 9 m x 9 m grid

A preliminary geomagnetic survey conducted by D Jacobs (personal communication, 2005) revealed unusually high magnetic fields over an area in the granulite terrain. In order to constrain the strength of these highly magnetized rocks L Carporzen (personal communication, 2005) collected palaeomagnetic data from holes drilled at 1 m intervals on 9 m x 9 m grid. In this region the surface rocks are composed solely of granite-gneiss.

The rocks also have a well defined metamorphic foliation trending toward the northwest (Fig. 4.14).

The geomagnetic field was measured at 0.55 m, 1.2 m and 2.5 m above each place where palaeomagnetic cores (see Chapter 5) were drilled, using sing the fluxgate magnetometer. The geomagnetic grid was extended by 2 m (relative to the palaeomagnetic grid) on all sides to avoid edge effects when modeling the geomagnetic data. Note that the orientation of the grid is rotated by 45º from the North (Fig. 4.15). Using the cesium magnetometer the 9 m x 9 m grid was extended 30 m to the SE and SW in order to study the lateral extent of the magnetic fields.

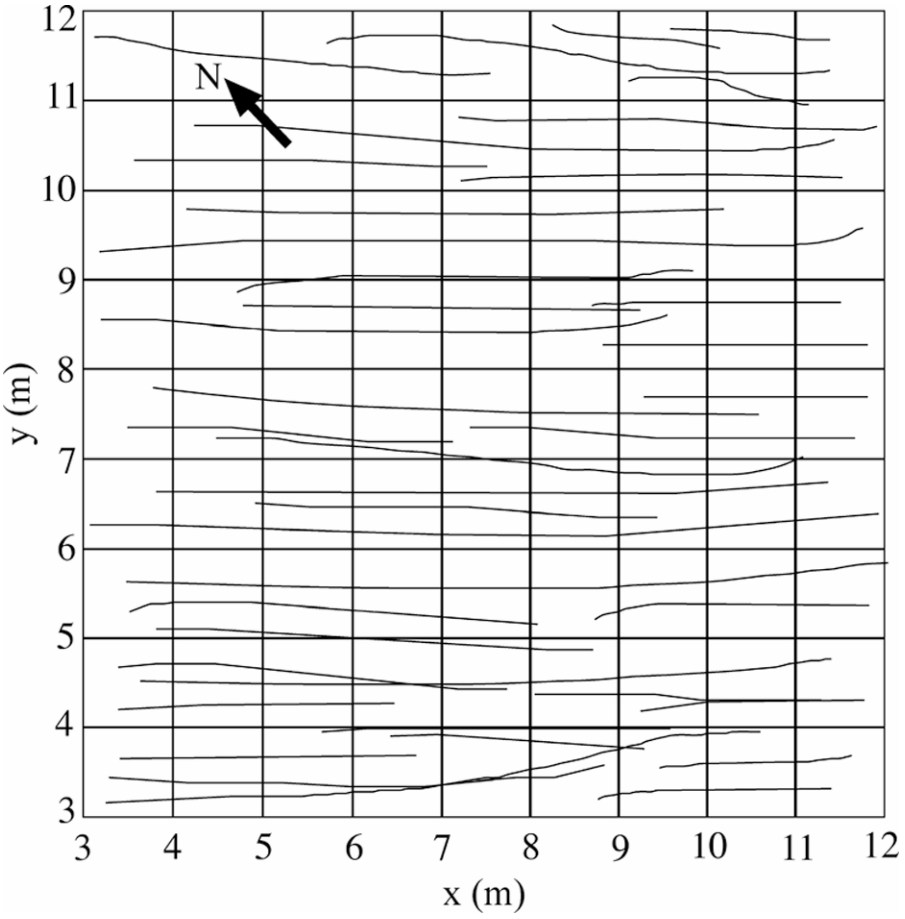

Figure 4.14. Metamorphic foliation across the 9 m x 9 m grid. Note the trend towards the NW.

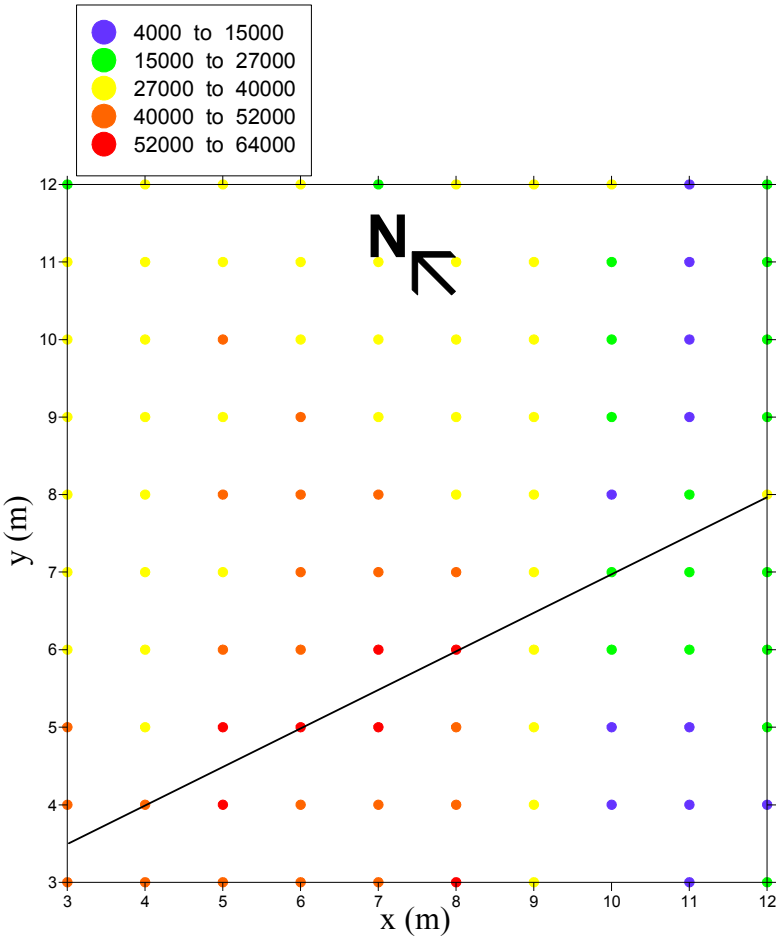

Figure 4.15. Magnetic survey over the 9 x 9 m grid used for the palaeomagnetic study in the granulites (station spacing 1 m, line spacing 1 m). Each point on this diagram represents the measured position and the corresponding raw magnetic values. Note that the scale in magnetic field is in nT. The straight line is the dyke mentioned in the text.

Figs. 4.16a-18a present the total IGRF corrected field anomaly while Figs. 4.16b-4.18b represent the vertical components of the magnetic field. The image at 0.55 m is characterised by a NE trending trough of very low magnetic field intensities that is almost equal to the present Earth's field (Fig. 4.16a). The average magnetic fields immediately parallel to the trough are double (56 000 nT) the Earth's field. This pattern is also observed at both 1.5 and 2.5 m heights (Figs. 4.17 and 4.18), although the amplitude of the anomalies diminishes by about 15 000 nT at 2.5 m.

The extended survey (Fig. 4.19) suggests that the negative trough continues in a SW direction for about 30 metres, and that it is as wide as 3 m in some places. The vertical magnetic component (as measured with the three component fluxgate magnetometer) over the trough has a polarity that is opposite to that of the total IGRF anomaly map (Figs. 4.16b, 4.17b and 4.18b respectively). By inference, this suggests that the direction of magnetization for the trough is opposite to that of the current earth's field. The position of the trough coincides with a high concentration of single domain magnetite and it also appears that the trough is perpendicular to the metamorphic foliation (Fig. 4.19).

The magnetic anomaly over the 9 m x 9 m grid suggests that it has a different source from the one causing the long wavelength anomaly (Figs. 4.2 and 4.4a) or is possibly due to enhanced magnetization. The latter has not been demonstrated as yet and this is the subject of Chapter 6, where modelling of this 9 m x 9 m grid will be undertaken with the view to placing constraints on shorter wavelength anomalies seen across the Vredefort basement and referred to in Section 4.2 above.

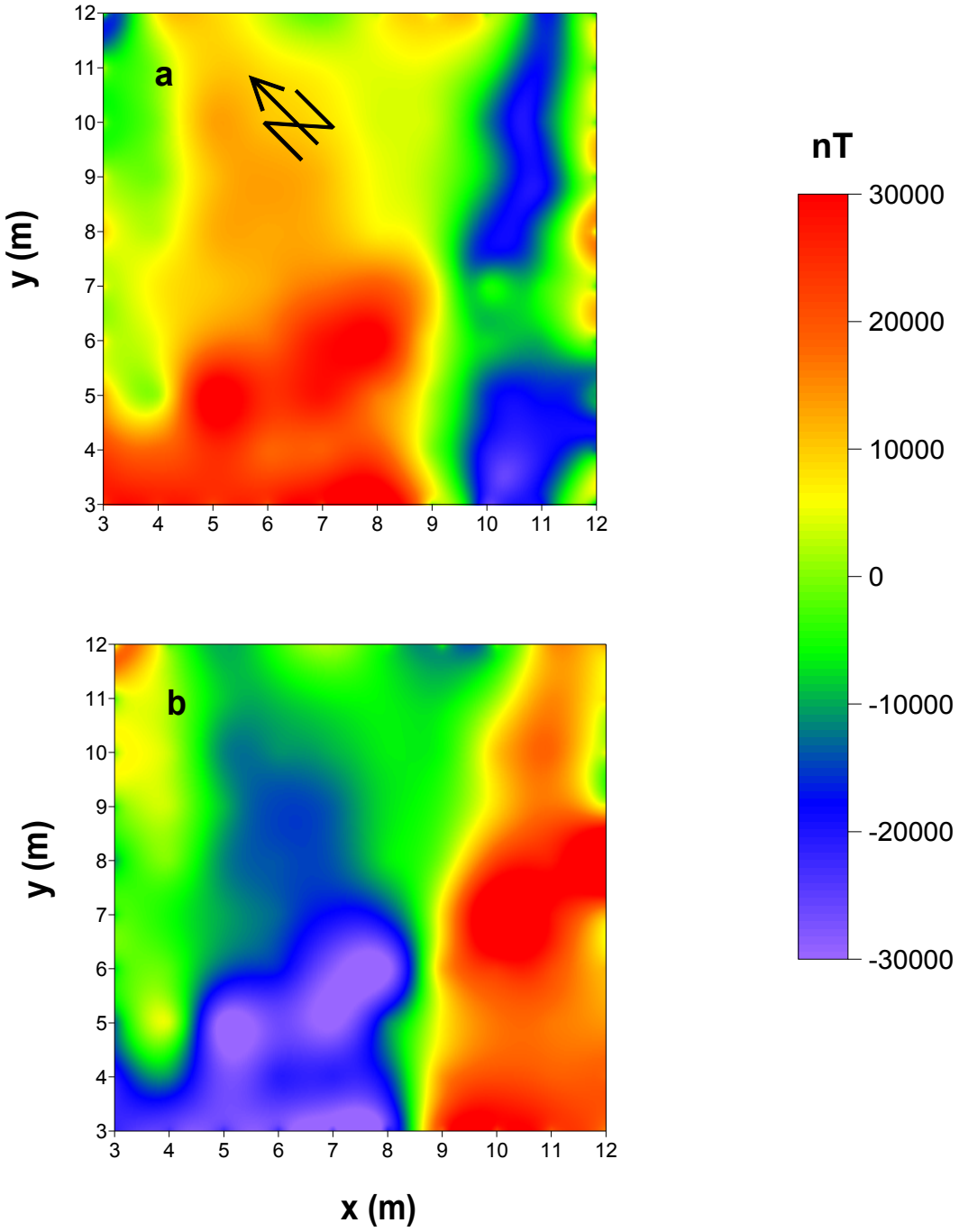

Figure 4.16. Magnetic images of the 9 m x 9 m grid in the granulites at a height of 0.55 m. a) IGRF corrected total magnetic anomaly map, b) IGRF corrected vertical magnetic anomaly map.

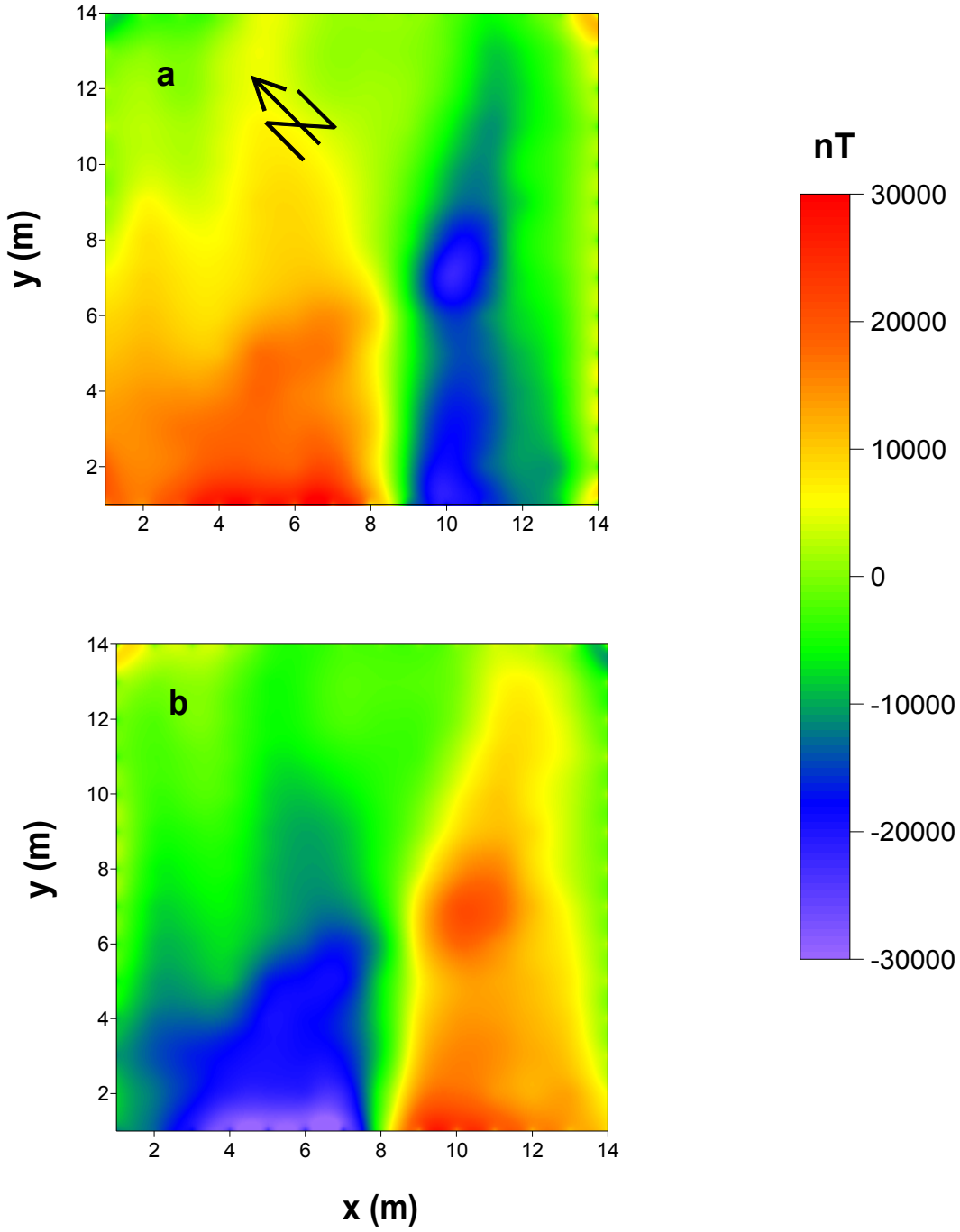

Figure 4.17. Magnetic images of the 9 x 9 m grid in the granulites at a height of 1.20 m. a) IGRF magnetic anomaly map, b) IGRF vertical magnetic anomaly map.

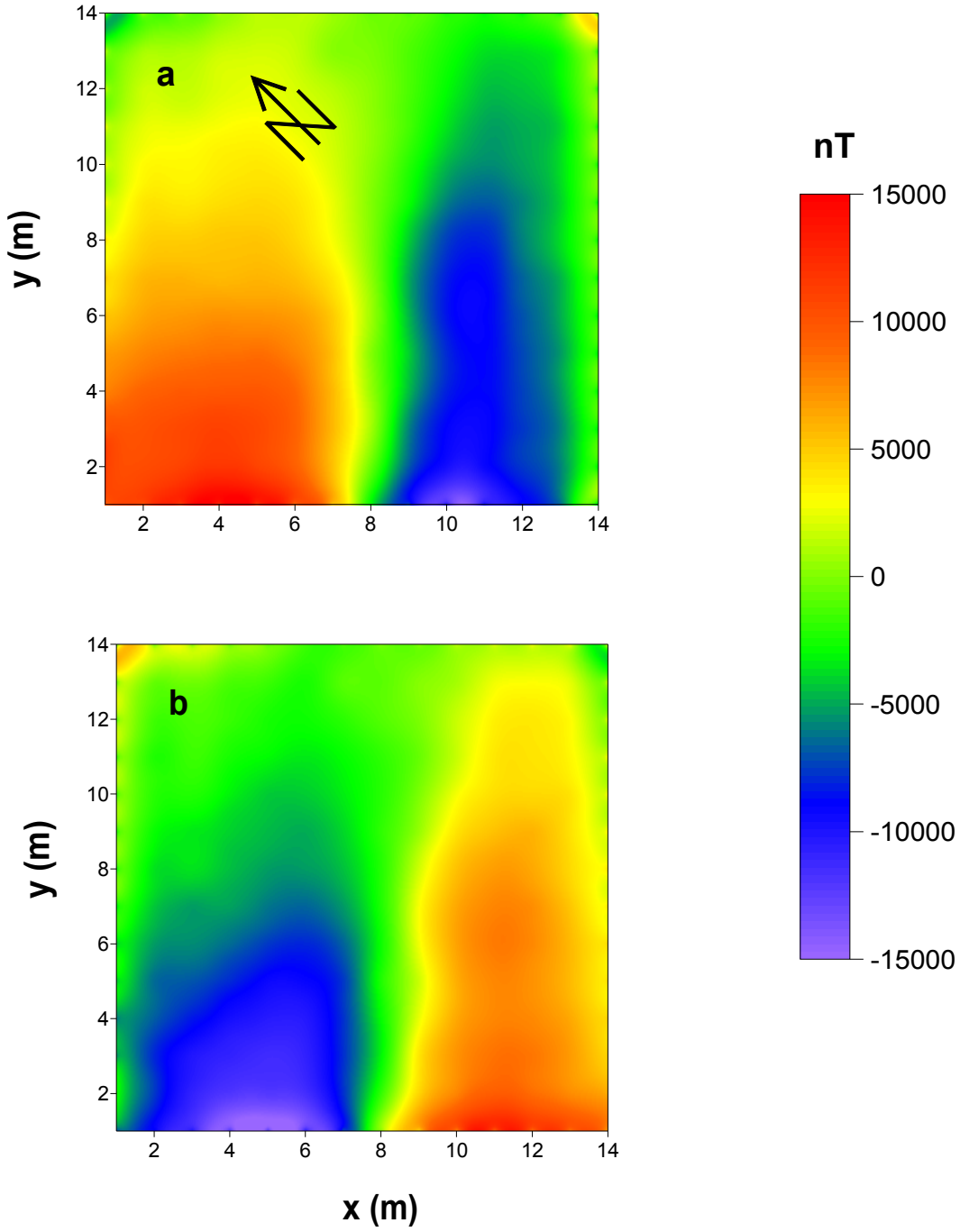

Figure 4.18. Magnetic images of the 9 x 9 m grid in the granulites at a height of 2.55 m. a) IGRF magnetic anomaly map, b) IGRF vertical magnetic anomaly map.

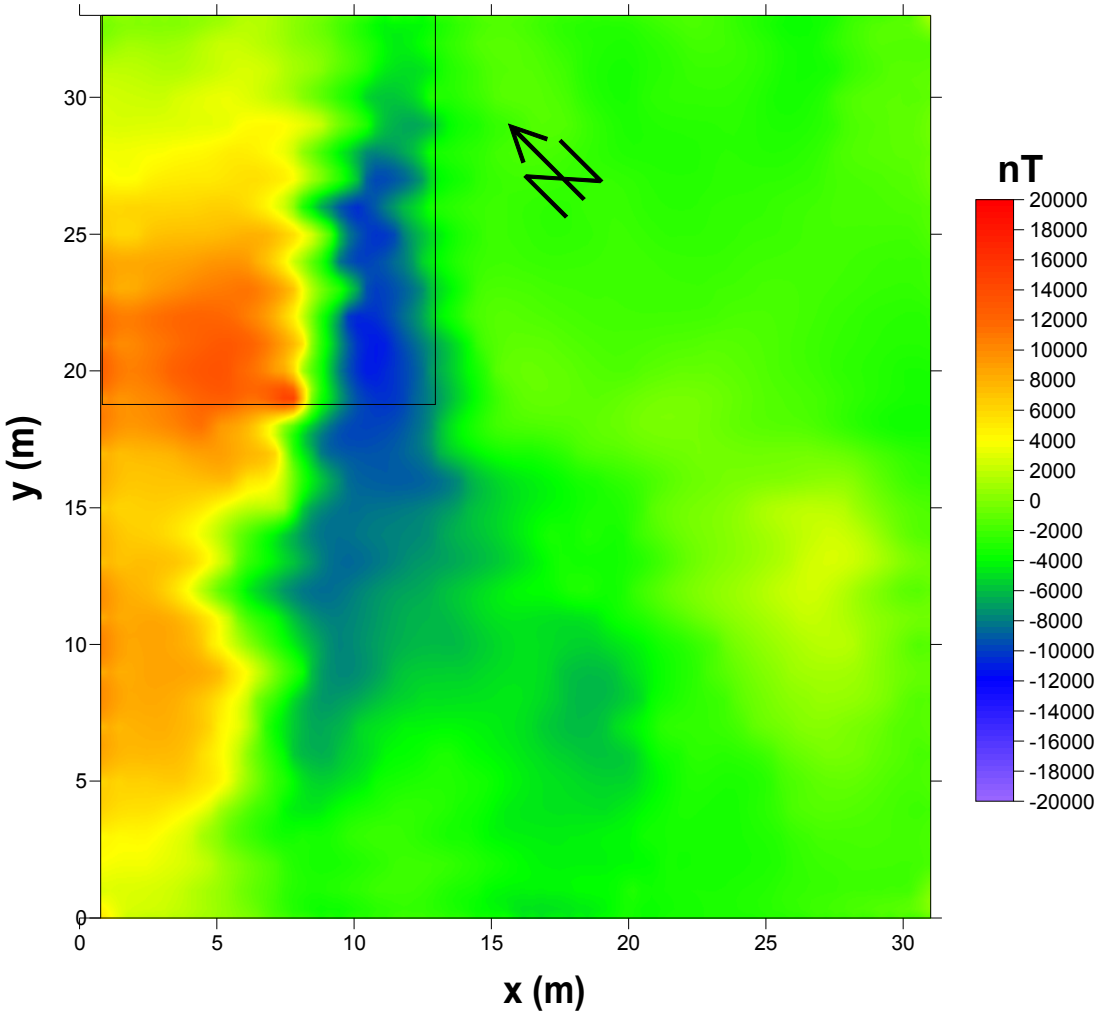

Figure 4.19. Extended survey over the 9 m x 9 m grid. Magnetic values measured with a cesium magnetometer at 2.5 m altitude. The top left square is the total geomagnetic field at 2.55 m altitude obtained from the fluxgate magnetometer survey (over 9 m x 9 m grid). The color scale ranges from – 20 000 nT to 20 000 nT in order to show up the contrasts in the map. The data was gridded to 0.25 m in both directions.

4.3 Interpretation and discussion of magnetic data

The results from this study show that detailed magnetic surveys can delineate the position of the amphibolite-granulite transition, as well as the radial and concentric faults that juxtapose the different geological units.

The data (upward continued to 150 m, Fig. 4.5c) from this study were found to be compatible with the aeromagnetic data over the same area. This implies that the association of the negative magnetic anomaly with the lithology can be extrapolated to the whole basement. Thus, from the aeromagnetic anomaly (Fig. 1.2, Chapter 1) it can be inferred that the amphibolite-granulite transition zone that was found to coincide with the north-west portion of the anomaly, extends over a circumference of 50 km around the entire central part of the crater. Seismic reflection profiles (Durrheim, 1986) across the central part of the Kaapvaal craton adjacent to the Vredefort structure, have revealed the presence of a seismic reflector in the Archaean crust at a depth of about 7.5 km beneath the Witwatersrand basin. This reflector has been attributed to a change of lithology or metamorphic grade (amphibolite-granulite transition zone) and it is interpreted as the Conrad discontinuity observed in some parts of the world (Wever, 1989). From this observation the author speculates (note that this was also made by other workers in the past) that the transition zone termed the "Vredefort discontinuity" is a regional feature that was uplifted and rotated into its present position during the impact event. It can therefore be concluded that the transition zone forms part of the central peak of a giant multi-ring crater (Reimold and Gibson, 1996) that has been uplifted to surface during the impact event, and that Vredefort is one of the rare places were the Conrad discontinuity can be studied on surface.

Application of AGC to the data suggests that there are a lot of subtle features and linear features which can be reasonably traced using this method. However, it is not easy to ascertain whether all the features seen in AGC maps have any geological association or not, as there are very little outcrops within the study area. Although the degree of success of the AGC method to the current study should not be overstated it is nevertheless a

powerful tool in the interpretation of magnetic data and this should be thoroughly used in any subsequent study focusing on the same area or adjacent areas.

Even if the south end of the NE-trending linear feature coincides with a water pipe there is no conclusive evidence that can link the anomaly directly to the pipe. (The author has not seen the pipe itself, but was only told of its possible existence). In particular the depth estimates of 18 m suggest that another source is possibly responsible for this anomaly, as it is highly unlikely for anyone to bury a water pipe at such depths. However, no cultural features are associated with the northern part of the linear feature and thus this part of the lineament remains unsolved.

The magnetic anomaly over the BIF is dominated by a positive anomaly surrounded by negative anomalies that indicate that the BIF must have been remagnetised or was not affected by the impact event. If the BIF's magnetization was not altered then one expects a predominant negative anomaly over it as seen over the basement rocks which also occur in the same area.

The anomaly over the 9 m x 9 m grid is characterized by a NE trending negative magnetic anomaly. The strength of the magnetic field is so high that at places it equals the earth's magnetic field and at other places it is double the earth's field. This trend is observed at the three different heights at which the magnetic field was measured, although the magnitude reduces drastically with each level of measurement. The shape of the trough continues for another 30 m to the southwest with a width of about 3 m. This suggests that the short wavelength anomalies are due to a different source compared with the long wavelength anomalies or they are possibly as a result of enhanced magnetization.